02

The simulation of proton beam passage through thin gold films

© *P.Yu. Babenko, A.N. Zinoviev, D.S. Tensin*

Ioffe Institute, St. Petersburg, Russia
e-mail: babenko@npd.ioffe.ru

Received June 8, 2022
Revised July 27, 2022
Accepted August 1, 2022

The results of calculating the energy spectra of protons transmitted and reflected from thin layers of gold are presented. The simulation results are compared with experimental data. It is shown that the stopping measurement results are affected by such factors as the multiple scattering, the geometry of the experiment, and the morphology and roughness of the target. An analysis of the angular dependence for particles passing through a thin film makes it possible to obtain information about the interaction potential between a particle and a solid. The obtained results on the potential agree with the data from experiments on the reflection of particles from the surface of a solid and differ markedly from the data on the potential determined from the scattering of particles in the gas phase.

Keywords: energy spectra, angular distribution, interatomic interaction potentials, electronic stopping, straggling.

DOI: 10.21883/TP.2022.11.55170.151-22

Introduction

Understanding the processes that occur when medium-energy particles (several keV) pass through thin layers of matter is very important for creating new materials using ion implantation methods. The use of energies lower than 10 keV allows to reduce the particle path in the substance and, therefore, reduces the size of the created nanostructures. Medium-energy beams of ions and atoms are widely used to analyze the composition and structure of surfaces. Modeling of the reflection, range, energy release, defect formation, and sputtering processes during ion beam bombardment is essential for a proper understanding of the interaction of plasma particles with the wall in a tokamak reactor and for modeling the effects of the solar wind on spacecraft.

When modeling the interaction of ions with a solid using computer codes, it is necessary to know the structure of the target, the interatomic interaction potential, the charge state of the interacting particles, and the nuclear and electronic energy losses during impact. The work of accumulating this data has been ongoing for many years. The binary collision approximation to speed up counting was proposed in [1]. A significant contribution to the development of modeling of particle scattering on the surface has been made by domestic authors [2–4]. Various surface modeling techniques are described in the monograph [5].

The SRIM [6], code, which is based on the use of the so-called universal potential, is widely used. The disadvantages of the code are that it is not possible to calculate scattering on crystalline and polycrystalline targets, and it is not possible to freely change the scattering potential and model, to account for inelastic energy losses during electron stopping. For modeling the calculation on a crystal target, we should mention the program MARLOWE [7], which is freely available. A number of attempts have been made to create programs for the polycrystalline target, which have not yet been widely [8–10]. The present work is motivated by the need to create code that is free of these disadvantages.

To verify the results, we chose the *p*-Au system for which numerous experimental data are available. Of recent works, we may note [11–14]. These papers present the results of a study of the passage of a medium-energy proton beam through thin layers of gold. The choice of gold is related to the possibility of obtaining thin films with minimal presence of impurity on the surface.

1. Simulating. Code description

We used a program developed by us that uses the Monte–Carlo method and the binary collision approximation to describe particle trajectories. In the binary collision approximation, the scattering of atomic particles in a solid is considered as a sequence of paired collisions with the atoms of the solid. In this case, the trajectory of particle motion is replaced by asymptotes of the trajectory. For impact energies below 50 eV the applicability of the approximation is violated. Approximation of binary collisions allows us to significantly speed up the calculations. In the present work up to 50 mln particle trajectories were analyzed, allowing good statistics in the analysis of the energy and angular distributions both for particles reflected from the surface and for particles that have passed through the thin film.

The developed program made it possible to perform calculations both for single-crystal and polycrystalline and amorphous targets. When modeling scattering on a crystal, the arrangement of atoms in space is given by the crystal lattice, with the surface given by a selected face of the crystal. When modeling scattering on a polycrystalline surface, the orientation of the surface face of the crystal is set randomly. The size of the crystallite is a parameter

of the problem. A surface is considered rough if there are irregularities with a value of the order of a lattice constant or more. When modeling scattering on an amorphous target, the presence of near-order is taken into account. The distance between atoms is determined from the density of the target. A densely packed cluster of atoms randomly oriented in space is specified. At the subsequent impact, the cluster orientation in space is played out anew. The surface is defined as a random slice of the original cluster. Roughness can be modeled by varying the film thickness.

A distinction is usually made between nuclear stopping, which is associated with scattering of the particle on the atoms of the target, and electronic stopping, which is associated with excitation and ionization, i. e., with interaction with the electronic component of the target. Energy losses from scattering on the lattice atoms are calculated accurately if the interaction potential is known. The energy loss in electronic stopping is taken into account for each impact by multiplying the theoretical value of the electronic stopping by the trajectory length between the collisions. The advantages of the program include the ability to vary the interaction potential and a model for describing the energy dependence of electronic stopping power. Thermal vibrations of the target atoms are taken into account. It is possible to build a surface map to analyze the area leading to the reflection of particles from the surface. The layer to which the particle reached is also fixed. A more detailed description of the algorithm can be found in [15].

2. Electronic stopping

Many papers have been devoted to the problem of properly accounting for electronic stopping in computer simulations [16–18]. There is a database [19] of experimental data on electronic stopping losses for various projectiles and targets. This database is constantly being updated with new data.

The values of inelastic energy loss for the system H−Au are taken by us from the works [12,13,20–23]. In the area of energies we are interested in, the experiment gives significantly different values of inelastic energy loss. The question arises: what values of inelastic loss to use in our program in the simulation?

The data obtained using backscattering geometry and the geometry on passage give different values of electronic stopping. An explanation for this phenomenon was found in our work [24]. It turned out that the multiplicity of collisions in the target plays a significant role. As our calculations have shown, the particle trajectory length L in matter at energies less than 10 keV is significantly greater than the thickness of the target d it passes (Fig. 1).

Fig. 2 shows the electronic stopping values from Markin [12] obtained by backscattering and from Andersen [14] measured when protons pass through a 200 Å thick gold film. It can be seen that Markin's data in the low-energy area are much lower than Andersen's data. When

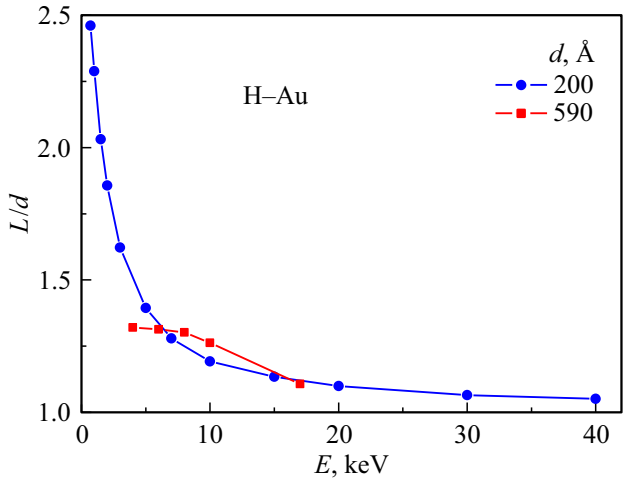

Figure 1. Ratio of average trajectory length L to film thickness d for the H−Au system for thicknesses of 200 and 590 Å.

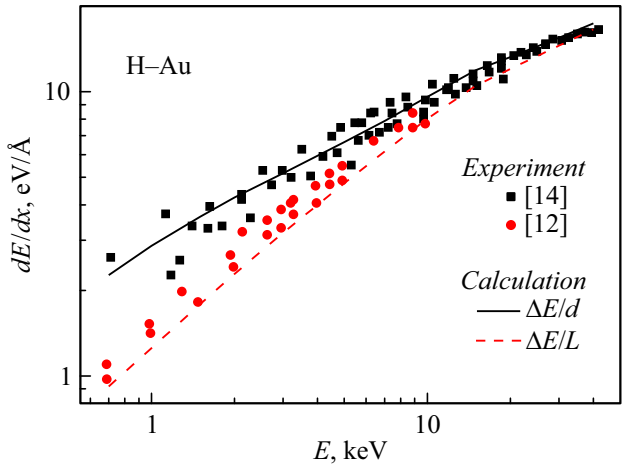

Figure 2. The values of the electronic stopping power dE/dx depending on the energy of the bombarding particle [24]. The points — experimental data of works [12,14]. Lines — our calculation of $\Delta E/d$ and $\Delta E/L$ values using the model [15].

we simulate the energy spectra of atomic particles passing through a 200 Å thick film with our program, we get the following result: If we divide ΔE — the average energy loss of particles passing the film by the film thickness d, we obtain Andersen [14] data, and if we divide the average energy loss by the average trajectory length L, we obtain Markin [12] results (Fig. 2).

Obviously, instead of the value „the energy loss per unit thickness of the target" should be used in the simulation, the parameter „the electronic stopping per unit trajectory length", and when comparing data from different experiments, a correction for multiple scattering should be made in the data obtained for thick films.

Experimental data obtained for thin films are more credible due to the lesser effect of multiple scattering. For example, the data in [20] were obtained for a film

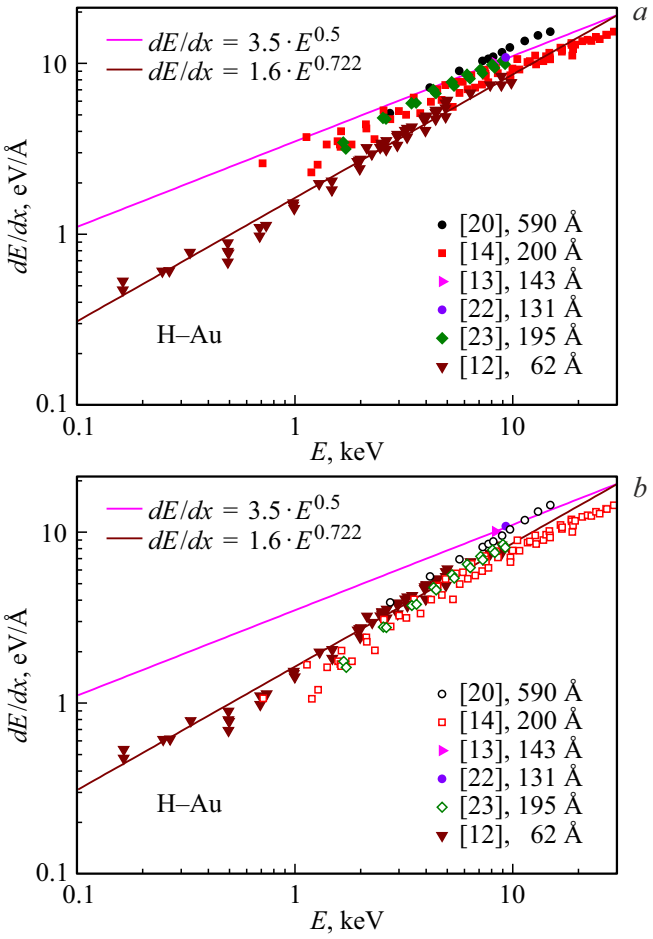

Figure 3. Dependence of the electron losses on the energy of the bombarding particle for protons in a gold target: *a* - without correction for multiple impact, *b* with correction.

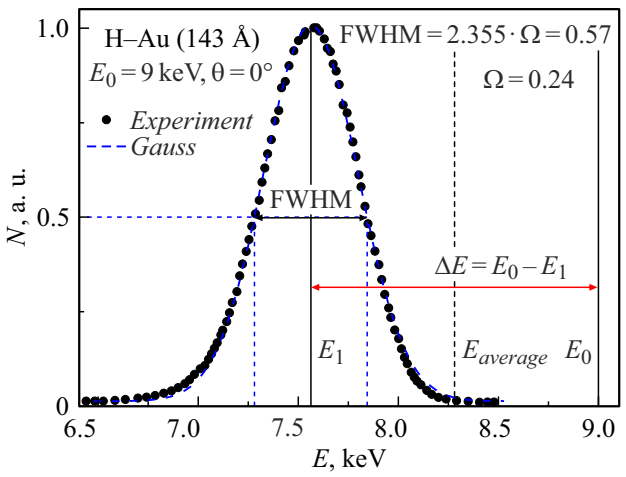

Figure 4. Energy spectrum of protons after passing through the gold film with a thickness of 143 Å. Initial energy of protons $E_0 = 9$ keV.

of 590 Åthickness, and we corrected for multiple scattering. The work [14] used particle acceleration and deceleration, which influenced the collection geometry of the particles that passed the film. In selecting the inelastic energy loss values, we gave more credence to the data obtained for films with thicknesses closer to 100 Å (143 Å [13], 131 Å [22]). In the work [23] the film thickness was 195 Å. As can be seen from Fig. 3, taking into account the multiple scattering correction markedly improves the agreement with the experimental data. This data set can be described by the dependence $dE/dx = 1.6 \cdot E^{0.722}$, which we will use later.

It should also be noted that the values of inelastic energy loss obtained from the experiment are given not for the initial energy of the bombarding particles, but for some average energy.

Figure 4 shows the experimental energy spectrum of protons passing through a thin gold target with a thickness of 143 Å. Observation angle $\theta = 0°$, energy of the flying protons $E_0 = 9$ keV. It is known that in the case of a thin target the energy spectrum of particles that have passed the film is described by the Gaussian distribution:

$$\frac{dN}{dE} = A \exp\left[-\frac{(E - E_1)^2}{2\Omega^2}\right]. \quad (1)$$

Here, E_1 — the average or most probable energy of the particles after passing through the film. The dashed line in Fig. 4 shows the Gaussian distribution that best describes the experiment. In further processing of the energy spectra on the shotgun, we will describe them by the Gaussian distribution and use the following parameters. Bombarding particle energy — E_0, average or most probable particle energy after passing the film — E_1, energy shift —$\Delta E = E_0 - E_1$, standard deviation in the Gaussian distribution — Ω.

A few words about the energy values for which inelastic losses are given. If E_0 — the initial energy of the particle, and E_1 — the average energy of the particle after passing through the film, then the arithmetic mean [14] value can be used to estimate the average particle energy during electronic stopping in a thin film:

$$E_{average} = \frac{E_0 + E_1}{2}. \quad (2)$$

If we assume that the electronic stopping changes with the energy of the particle according to the law $dE/dx = AE^{\sigma}$ (the curve in Fig. 3), then for the average energy we can get the expression

$$E(\sigma) = \frac{(1-\sigma)}{(1+\sigma)} \frac{(E_1^{2-\sigma} - E_0^{2-\sigma})}{(E_1^{1-\sigma} - E_0^{1-\sigma})}. \quad (3)$$

For the frequently used approximation c $\sigma = 0.5$:

$$E(\sigma = 0.5) = \frac{1}{3}(E_0 + E_1 + E_1^{0.5} E_0^{0.5}). \quad (4)$$

Fig. 5 shows that the values for the different models do not differ significantly. For thin films, it is more convenient to use the arithmetic mean value, while for thicker films we propose to use the expression (3) obtained by us.

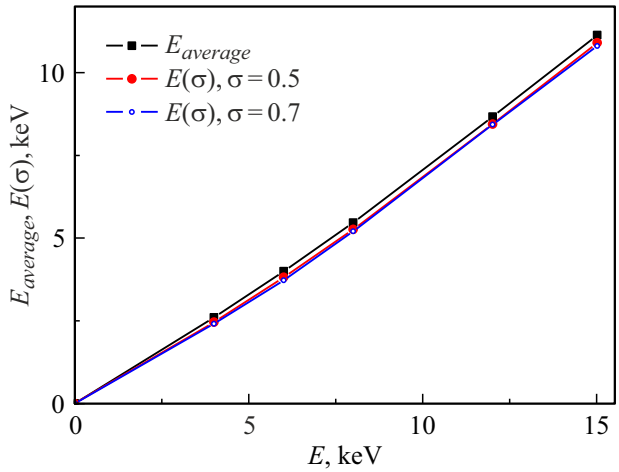

Figure 5. Dependence of average particle energy on projectile particle energy for three variants of calculation: arithmetic mean and our proposed formula for $\sigma = 0.5$ and 0.7. Film thickness $d = 590$ Å.

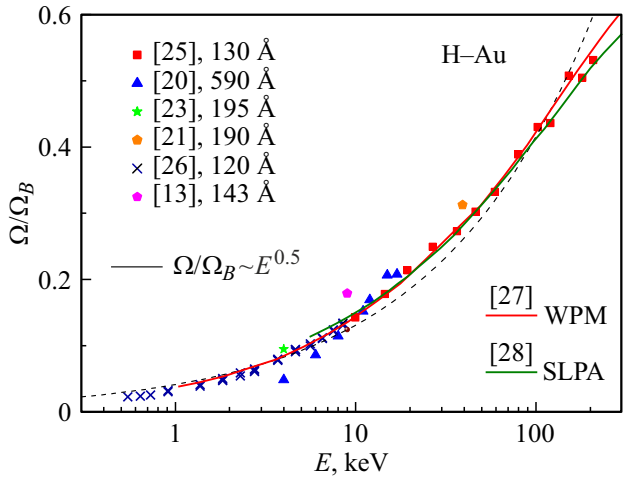

Figure 6. Dependence of straggling on the energy of flying particles. Dots — experimental data. Lines — degree dependence and theoretical calculation from [27,28] work.

3. Energy straggling

When modeling the energy spectra after thin films in the previously used versions of the program, the spectra were obtained asymmetrical and with a sharp high-energy right edge. This energy distribution takes into account only the elastic energy loss due to multiple scattering on the lattice atoms. It is also necessary to take into account the random nature of the energy loss when stopping the particles (straggling) on the target electrons. This energy straggling is due to the random nature of the charge state of the flying particle, as well as to the non-uniform distribution of the electron density in the target.

Roughness (uneven film thickness) can also contribute to the broadening of the peak in the energy spectrum. The measurable peak width is also affected by the energy resolution of the spectrometer used to analyze the particles.

The energy-loss distribution has a Gaussian form, provided that the energy transfer in an individual collision is less than the width of the total distribution. The standard deviation Ω in the Gaussian distribution is expressed by the formula

$$\Omega^2 = Nd \int T^2 \, d\sigma(T). \qquad (5)$$

Here, N - atomic density of the target, d — thickness of the target, T —energy transfer, $d\sigma$ — differential scattering cross section. For fast particles, the expression for the straggling is well approximated by the Bohr formula:

$$\Omega_B^2 = 4\pi Z_1^2 e^4 Z_2 Nd, \qquad (5)$$

which is obtained by substituting Rutherford's formula for the cross section into formula (5). Here, Z_1 and Z_2 — atomic number of the projectile and target, respectively.

Fig. 6 shows the experimental straggling values for the H−Au system from the works [13,20,21,23,25,26]. Using the ratio Ω/Ω_B allows you to compare measurement data for different target thicknesses. The entire data set is described by the power relation $\Omega/\Omega_B \sim E^{0.5}$. The assumption that the magnitude of the straggling is proportional to the velocity of the particle is based on the results of theoretical work [27,28] (Fig. 6). It can be seen that the theoretical curves describe the existing experimental data well.

Using the experimental data on straggling in the interaction of protons with a gold target, we have a module in our code that takes straggling into account. Straggling was taken into account in the simulation as follows: a term was added to the value of energy loss between collisions, the value of which was randomly played with a Gaussian distribution, and Ω was chosen from the fit of the resulting data to the curve in Fig. 6.

4. Dependence of inelastic loss on the observation angle

Fig. 7 shows the experimental spectrum of protons passing the gold foil with a thickness of 143 Å [13]. The energy of the flying protons — 9 keV. The data are given for two observation angles $\theta = 0$ and 20°. It can be seen that there is a shift in the position of the peak on the energy scale, depending on the particle observation angle. The peak shift is associated with an increase in the length of the particle trajectory with an increase in the escape angle. If we accept the model that the particle experiences many small-angle deflected collisions and at least one large-angle deflected collision of the order of θ, then, the average increase in span length with changes in the observation angle is described by the simple expression

$$\frac{1}{2}\left(\frac{1}{\cos\theta} - 1\right). \qquad (7)$$

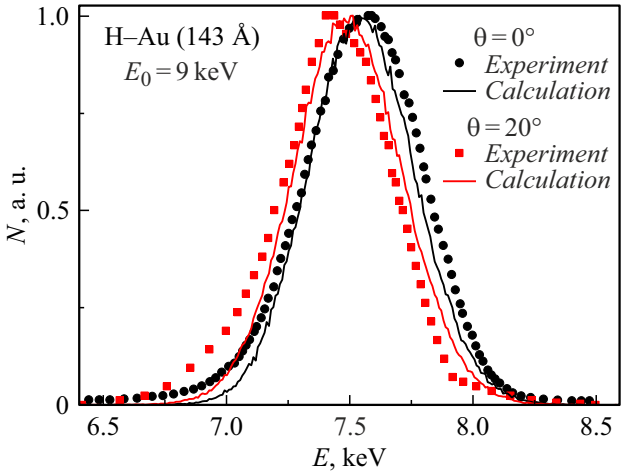

Figure 7. Energy spectra of protons passing through a gold film with a thickness of 143 Å. The energy of the incoming protons $E_0 = 9$ keV. Observation angles $\theta = 0$ and 20°. The points — experiment from the [ ]13 work, the lines — calculated by our program.

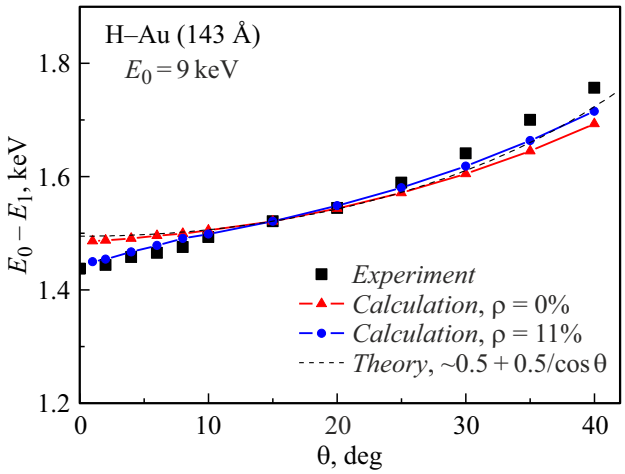

Figure 8. Dependence of the energy shift ΔE on the observation angle. Squares — experiment from work [13]. Triangles — our calculation without regard to roughness. The dashed line — dependence reflecting the increase in the run length as a function of the observation angle. Circles — calculation for the roughness parameter $\rho = 11\%$.

Under this assumption, the change in the electronic stopping losses depending on the angle of observation can be written in the form of

$$\Delta E_{elec}(\theta) - \Delta E_{elec}(0) = \frac{1}{2}\left(\frac{1}{\cos\theta} - 1\right)\Delta E_{elec}(0). \quad (8)$$

where $\Delta E_{elec}(0)$ — electron energy loss measured for zero observation angle.

The peak position is also affected by the position of the elastic peak at a given angle of scattering. The contribution of collision losses with nuclei (elastic losses) for $M_1 \ll M_2$ is approximately

$$\Delta E_{nucl}(\theta) - \Delta E_{nucl}(0) \cong \Delta E_{nucl}(\theta) \cong 4\,\frac{M_1 M_2}{(M_1 + M_2)^2} \times E \sin^2\left(\frac{\theta}{2}\right). \quad (9)$$

In our case of proton scattering on a gold target, this correction is small because of the strong difference of masses M_1 and M_2, for example for the scattering angle $\theta = 30°$ the value of $\Delta E_{nucl} \approx 1/200\,E$.

Energy loss is a function of observation angle. The angular resolution of the detector determines the magnitude of the energy spectrum shift. When analyzing the experimental data, it should be taken into account that the collection angle of scattered ions will affect the determined value of inelastic energy loss. For example, the measurments in the Andersen [14] experiment could be due to the fact that additional acceleration and deceleration of the particle beam passing the film was used for particle collection, which could affect the particle collection geometry and consequently the measurement uncertainty.

Fig. 8 shows that the experimental value of ΔE exceeds the calculated value. A simple model that takes into account only the increase in trajectory length as the observation angle increases (dashed line) satisfactorily describes our computer calculation. However, there is no complete agreement between the calculation and the experiment, and taking roughness into account improves the agreement. The method for calculating the effect of roughness on the observed shear ΔE will be discussed in the next section.

5. Influence of film roughness on measured values

This phenomenon has been pointed out in the works [13,29]. Obviously, the roughness of the film or its thickness variation should lead to an increase in straggling. According to [30]:

$$\Omega = \sqrt{\Omega_0^2 + \left(\frac{dE}{dx}\right)^2 \sigma_x^2} \cong \sqrt{\Omega_0^2 + \rho^2 \Delta E^2}. \quad (10)$$

Here, Ω_0 — the energy straggling of an ideal film thickness d, σ_x — the standard relative thickness deviation, ΔE — the energy loss and ρ - the roughness parameter characterizing the target thickness, which is defined as $\rho = \sigma_x/d$.

We estimated the effect of roughness for the parameter $\rho = 11\%$. It is possible to calculate the energy spectrum of particles passing through the film for a different set of thicknesses, and then add up the resulting spectra observed at different angles $\theta = 1{-}40°$, taking into account the weight contribution of different film thicknesses for different

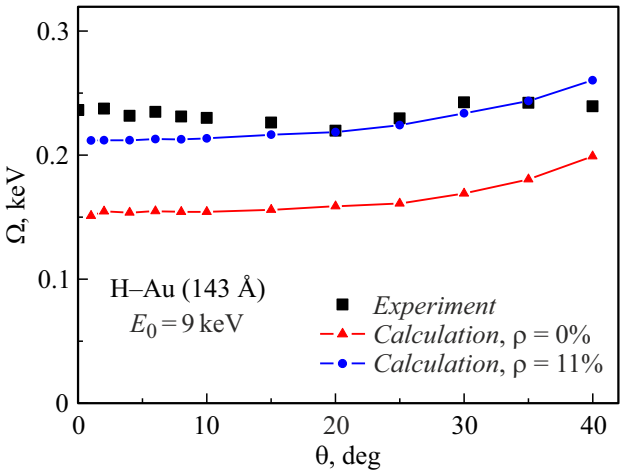

Figure 9. Straggling depending on the observation angle. Squares — experiment from work [13]. Triangles — our calculation without regard to roughness. Circles — calculation for the roughness parameter $\rho = 11\%$.

roughnesses. The energy spectrum for a target with a thickness spread was calculated using the formula

$$\left(\frac{dN}{dE}\right)_{\Sigma} = \sum_{i=1}^{9}\left(\frac{dN}{dE}\right)_{i} k_i. \qquad (11)$$

Here, $(dN/dE)_i$ - the energy spectrum for i-thickness, k_i - the weight factor of a given film thickness. The total spectra for different observation angles were processed using the standard procedure (fitting a Gaussian distribution). From the calculated spectra, the positions of the peaks of the most probable energy of the particles that have passed the film and the width of the Gaussian distribution (straggling) were obtained. Taking roughness into account leads to an additional shift of the peak corresponding to the average energy loss (Fig. 8). This phenomenon is related to the nonlinearity of the dependence of the particle scattering probability on the angle and thickness of the film.

Fig. 9 shows the values of the widths of energy distributions (straggling) for the experimental spectra and calculations with $\rho = 0$ and 11%. The figure shows that the calculated values of straggling without regard to roughness are significantly less than the experimental values, and with regard to roughness the agreement with the experiment is achieved.

The peak positions for the roughness parameter $\rho = 11\%$ were obtained in the same way (Fig. 8). It can be seen that taking into account the roughness of the film improves the agreement with experiment.

6. Angular distributions of particles that have passed through thin films

For practical purposes, angular distributions of the intensities of particles that have passed through thin films are often needed. For example, thin films are used to ionize a beam of neutral particles for their subsequent analysis [31].

Experimental conditions from work [13,32]

Work	Energy proton E_0, keV	Target type	Thickness target, Å
[13]	9	Polycrystalline	143
[32]	10	Polycrystalline	153
[32]	10	Monocrystalline	100

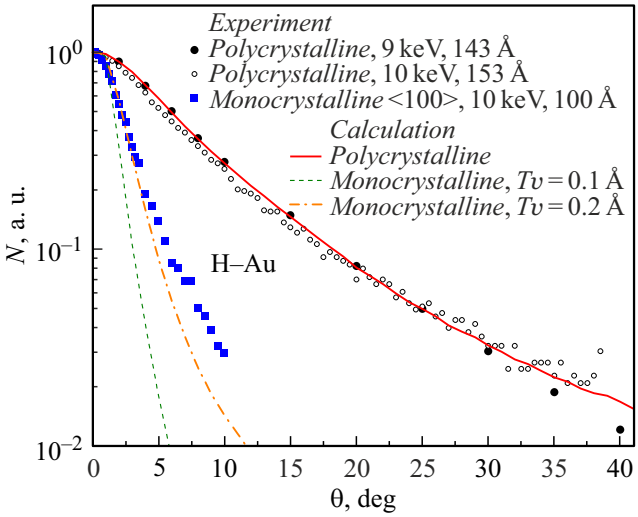

Figure 10. Angular distributions of protons after the passage of gold films. Points — experiment for polycrystalline and monocrystalline film. Lines — calculated by our program.

In [13,32], experimental data on the angular distribution of protons after passing through a gold film are given. The table summarizes the experimental conditions under which measurements were made in these works.

Fig. 10 shows the experimental angular distributions of protons after passing through the gold films. The data for polycrystalline targets from various papers agree well. You can see that the angular distribution for the monocrystal is much narrower. In order to obtain agreement between calculation and experiment in the case of monocrystals, we had to use the amplitude of thermal vibrations $Tv = 0.2$ Å, and this value is twice the amplitude of the vibrations calculated from the Debye temperature $Tv = 0.089$ Å. The discrepancy in the results may be due to the presence of defects in the monocrystalline film. As can be seen from Fig. 10, our program describes the experiment quite well.

7. Getting data on the potential of interatomic interaction

When modeling the processes of interaction of particles with matter, the choice of the interatomic interaction potential is essential. Studies show that the angular

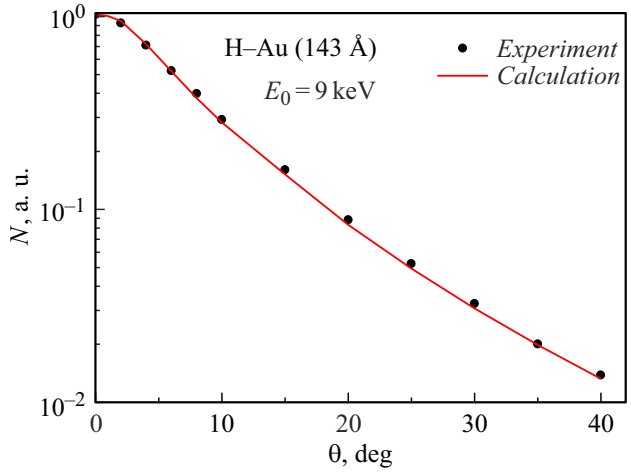

Figure 11. Angular distribution of protons after passing through the gold film. Dots — experiment for polycrystalline film. Line — calculating with our program.

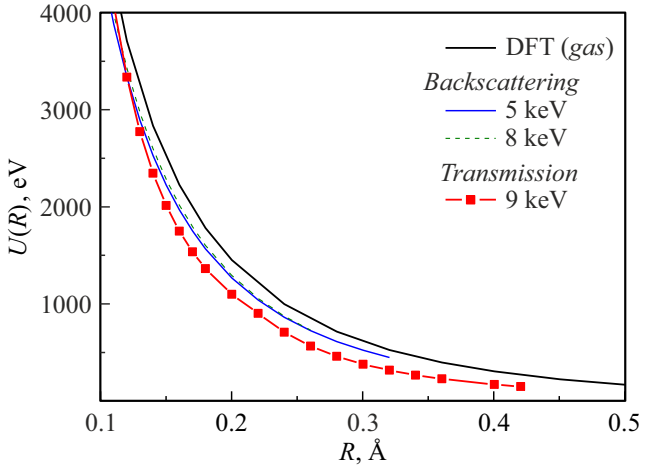

Figure 12. Interatomic interaction potentials obtained by fitting an angular distribution to measurements from work [13].

distribution of scattered particles is very sensitive to the interaction potential. Consequently, by modeling the angular distribution of particles after the passage of thin layers of matter, it is possible to select the interatomic interaction potential.

As can be seen from Fig. 11, the experimentally observed dependence of the scattering intensity on the observation angle can be well described by selecting the interaction potential. The best agreement was obtained for the potential:

$$U(R) = \left\{ \begin{array}{ll} \dfrac{13}{R^{2.8}} & \text{if} \quad R > 0.22, \\ \dfrac{13}{R^{2.8}} \exp\left[-4(0.22 - R)\right] & \text{if} \quad R < 0.22 \end{array} \right\}. \tag{12}$$

Fig. 12 shows the interaction potentials obtained in the present work, which agree well with the data obtained from the analysis of the energy and angle dependences of the particle reflection coefficients during proton bombardment of thick gold targets. At the same time, it is confirmed that the potential for the atom–solid system is markedly different from the data obtained by scattering particles in the gas phase (curve DFT). Due to the high mobility of electrons in the metal, the passing particle can polarize the electron gas, which can lead to a change in the screening constant in the potential.

8. Energy spectra per reflection

Section 8 shows the results of calculating the energy spectra of protons reflected back (at large angles) from thin layers of matter.

Figure 13 shows the calculation for a film thickness of 62 Å and proton energy of 700 eV. It can be seen that the

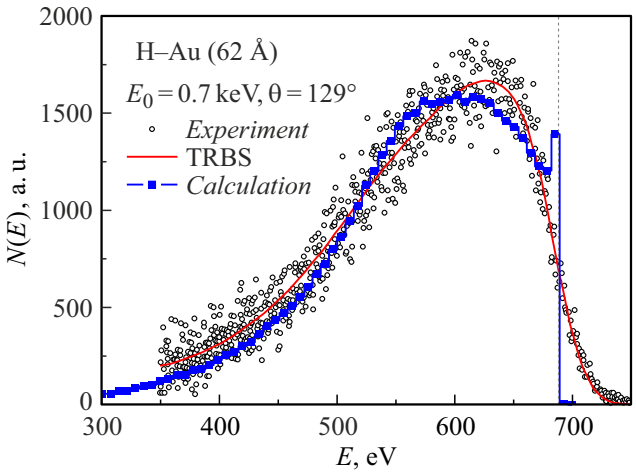

Figure 13. Energy spectrum of protons scattered from a gold target at an angle of 129°. Circles — experimental data from work [12]. The solid line — -the TRBS calculation from work [12].. Squares — calculating with our program.

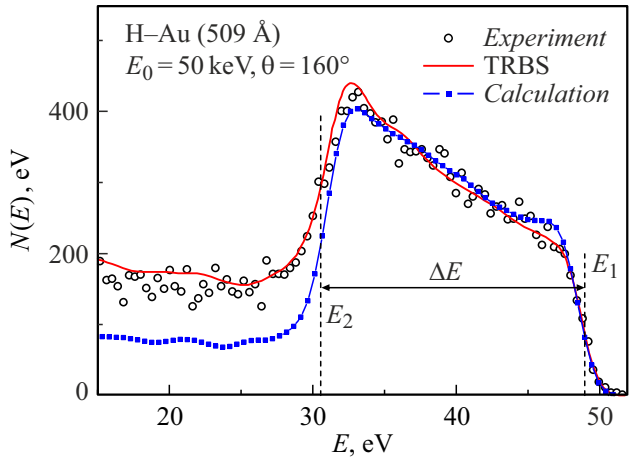

Figure 14. Energy spectrum of protons scattered from a gold target at an angle of 160°. Circles — experimental data from work [11]. The solid line — -the TRBS calculation from work [11]. Squares — calculating with our program.

simulation by our program gives a feature in the spectrum related to proton scattering at an angle 129° on the surface layer of the film.

Fig. 14 shows the energy spectrum of protons reflected back at an angle of $\theta = 160°$ from a gold layer of thickness $d = 509$ Å. The spectrum obtained with the TRBS [33] computer simulation and our program is also given. The best description of the experimental spectrum by the TRBS code is achieved for the inelastic energy loss value $(dE/dx)_{\mathrm{TRBS}} = 17.8$ eV/Å. The experimental spectrum shows two sharp edges (labeled in the figure as E_1 and E_2). The energy E_1 corresponds to the particles reflected from the uppermost layer of the film, and the energy E_2 — particles reflected from the deepest layer. To get an estimate of the electronic stopping, you must divide $\Delta E = E_1 - E_2 = 18\,430$ eV by the path of the particle $L = d + d/\cos(180° - \theta)$. Here, d — thickness of the film (509 Å), θ scattering angle equal to 160°. Hence, $L = 1051$ Å. The estimated value $dE/dx \approx 17.5$ eV/Å is in excellent agreement with the computer simulation results.

Thus, for different film thicknesses and energies, our code allows us to calculate the energy spectra of particles scattered both forward and backward.

Conclusion

This paper presents the results of computer simulations of the energy spectra of particles that have passed through thin layers of matter. The simulation was performed using a code based on the Monte−-Carlo method and the binary interaction approximation. The code allows different types of interatomic interaction potentials to be applied to calculations, the structure of the target (amorphous body, polycrystal, crystal) to be modeled, the amplitude of thermal vibrations of target atoms to be considered, and the energy straggling of particles to be introduced.

The paper takes into account the energy straggling and verifies the applicability of the code in two significantly different geometries for the shot and backscattering. It is shown that when interpreting particle scattering data, the morphology of the target (monocrystal, polycrystal, amorphous body) must be taken into account. The results of energy loss measurements are affected by multiple scattering, particle collection geometry, and target roughness, which correct for the determination of inelastic energy losses. In modeling the angular scattering of particles, the interatomic interaction potentials were obtained. The potential data for the shoot-through geometry and backscattering are in good agreement. At the same time, there is a noticeable difference in the potential for the atom−solid system from the data obtained by scattering particles in the gas phase. This behavior may be due to a change in the screening constant in the potential due to the high mobility of the electron gas in the metal and polarization of the electron gas by a passing particle.

Financial support of work

The study was supported by a grant from the Russian Science Foundation № 22-22-20081 (https://rscf.ru/project/22-22-20081/) and supported by a grant from the St. Petersburg Science Foundation in accordance with the agreement dated„14“ April 2022 № 22/2022.

Conflict of interest

The authors declare that they have no conflict of interest.

References

[1] M.T. Robinson, I.M. Torrens. Phys. Rev. B, **9** (12), 5008 (1974). DOI: 10.1103/PhysRevB.9.5008
[2] V.M. Kivilis, E.S. Parilis, N.Yu. Turaev. DAN, **173** (4), 805 (1967).
[3] V.E. Yurasova, V.I. Shulga, D.S. Karpuzov. Can. J. Phys., **46** (6), 759 (1968). DOI: 10.1139/p68-094
[4] E.S. Mashkova, V.A. Molchanov, *Primenenie rasseyaniya ionov dlya analiza tverdykh tel* (Energoatomizdat, M., 1995), 176 p.
[5] W. Eckstein. *Computer Simulation of Ion-Solid Interactions* (Springer, Berlin 1991)
[6] J.F. Ziegler, J.P. Biersack. SRIM. Available at: http://www.srim.org
[7] Electronic source. Available at: http://www.oecd-nea.org/tools/abstract/detail/psr-0137
[8] G.E. Thomas, L.J. Beckers, J.J. Vrakking, B.R. Koning. J. Cryst. Growth, **56** (3), 557 (1982). DOI: 10.1016/0022-0248(82)90039-2
[9] M. Hautala. Phys. Rev. B, **30** (9), 5010 (1984). DOI: 10.1103/PhysRevB.30.5010
[10] I. Koponen, M. Hautala. Nucl. Instr. Meth. Phys. Res. B, **33** (1–4), 112 (1988). DOI: 10.1016/0168-583X(88)90525-3
[11] B. Bruckner, P.M. Wolf, P. Bauer, D. Primetzhofer. Nucl. Instr. Meth. Phys. Res. B, **489**, 82 (2021). DOI: 10.1016/j.nimb.2020.08.005
[12] S.N. Markin, D. Primetzhofer, S. Prusa, M. Brunmayr, G. Kowarik, F. Aumayr, P. Bauer. Phys. Rev. B, **78** (19), 195122 (2008). DOI: 10.1103/PhysRevB.78.195122
[13] M. Fama, G.H. Lantschner, J.C. Eckardt, C.D. Denton, N.R. Arista. Nucl. Instr. Meth. Phys. Res. B, **164**–**165**, 241 (2000). DOI: 10.1016/S0168-583X(99)01086-1
[14] H.H. Andersen, A. Csete, T. Ichioka, H. Knudsen, S.P. Moller, U.I. Uggerhoj. Nucl. Instr. Meth. Phys. Res. B, **194**, 217 (2002). DOI: 10.1016/S0168-583X(02)00692-4
[15] D.S. Meluzova, P.Yu. Babenko, A.P. Shergin, A.N. Zinoviev, J. Surf. Invest.: X-ray, Synchrotron Neutron Tech., **13**, 335 (2019). DOI: 10.1134/S1027451019020332
[16] H. Paul, A. Schinner. Phys. Scripta, **69**, C41 (2004). DOI: 10.1238/Physica.Regular.069a00C41
[17] P. Sigmund, A. Schinner. Nucl. Instr. Meth. Phys. Res. B, **410**, 78 (2017). DOI: 10.1016/j.nimb.2017.08.011
[18] D. Goebl, K. Khalal-Kouache, D. Roth, E. Steinbauer, P. Bauer. Phys. Rev. A, **88** (3), 032901 (2013). DOI: 10.1103/PhysRevA.88.032901
[19] Electronic source. NDS — data base. Available at: https://www-nds.iaea.org

[20] R. Blume, W. Eckstein, H. Verbeek. Nucl. Instr. Meth., **168** (1–3), 57 (1980). DOI: 10.1016/0029-554X(80)91231-8
[21] K. Morita, H. Akimune, T. Suita. J. Phys. Soc. Jpn., **25** (6), 1525 (1968). DOI: 10.1143/JPSJ.25.1525
[22] C.D. Archubi, J.C. Eckardt, G.H. Lantschner, N.R. Arista. Phys. Rev. A, **73** (4), 042901 (2006). DOI: 10.1103/PhysRevA.73.042901
[23] J.E. Valdes, G. Martínez-Tamayo, G.H. Lantschner. J.C. Eckardt, N.R. Arista. Nucl. Instr. Meth. Phys. Res. B, **73** (3), 313 (1993). DOI: 10.1016/0168-583X(93)95744-P
[24] A.N. Zinoviev, P.Yu. Babenko. Pis'ma v ZhETF, **115** (9) 603 (2022). DOI: 10.31857/S1234567822090105
[25] J.C. Eckardt, G.H. Lantschner. Nucl. Instr. Meth. Phys. Res. B, **175**–**177**, 93 (2001). DOI: 10.1016/S0168-583X(00)00623-6
[26] E.A. Figueroa, E.D. Cantero, J.C. Eckardt, G.H. Lantschner, N.R. Arista. Phys. Rev. A, **75** (6), 064902 (2007). DOI: 10.1103/PhysRevA.75.064902
[27] C.D. Archubi, N.R. Arista. Phys. Rev. A, **96** (6), 062701 (2017). DOI: 10.1103/PhysRevA.96.062701
[28] C.C. Montanari, C.D. Archubi, D.M. Mitnik, J.E. Miraglia. Phys. Rev. A, **79** (3), 032903 (2009). DOI: 10.1103/PhysRevA.79.032903
[29] M.M. Jakas, N.E. Capuj. Nucl. Instr. Meth. Phys. Res. B, **36**, 491 (1989). DOI: 10.1016/0168-583X(89)90354-6
[30] F. Besenbacher, J.U. Andersen, E. Bonderup. Nucl. Instr. Meth., **168**, 1 (1980). DOI: 10.1016/0029-554X(80)91224-0
[31] S.Ya. Petrov, V.I. Afanasyev, A.D. Melnik, M.I. Mironov, A.S. Navolotsky, V.G. Nesenevich, M.P. Petrov, F.V. Chernyshev, I.V. Kedrov, E.G. Kuzmin, B.V. Lyublin, S.S. Kozlovski, A.N. Mokeev. Phys. Atom. Nucl., **80** (7), 1268 (2017). DOI: 10.1134/S1063778817070109
[32] C. Archubi, C. Denton, J.C. Eckardt, G.H. Lantschner, F. Lovey, J. Valdes, C. Parra, F. Zappa, N.R. Arista. Phys. Stat. Sol. B, **241**, 2389 (2004). DOI: 10.1002/pssb.200304862
[33] J.P. Biersack, E. Steinbauer, P. Bauer. Nucl. Instr. Meth. Phys. Res. B, **61**, 77 (1991). DOI: 10.1016/0168-583X(91)95564-T